Rev. Adv. Mater. Sci. 35 (2013) 75-85

# PHYSICAL SIMULATION OF COLD ROLLING OF ULTRA-FINE GRAINED AL 5083 ALLOY TO STUDY MICROSTRUCTURE EVOLUTION

**M.Yu. Murashkin[1,2], N.A. Enikeev[1,2], V.U. Kazykhanov[2], I. Sabirov[3] and R.Z. Valiev[1,2]**

[1]Laboratory for Mechanics of Bulk Nanostructured Materials, Saint Petersburg State University, Universitetsky pr. 28, 198504, Peterhof, Saint Petersburg, Russia
[2]Institute for Physics of Advanced Materials, Ufa State Aviation Technical University, K. Marx str. 12, Ufa, 450000, Russia
[3]IMDEA Materials Institute, Calle Eric Kandel 2, Getafe, 28906, Madrid, Spain

*Received: November 06, 2013*

**Abstract.** Recent investigations have demonstrated that ultra-fine grained (UFG) Al 5xxx alloys have a significant potential for industrial applications due to their enhanced mechanical and functional properties. The Al 5xxx alloys often have to undergo hot/cold rolling metalforming operations for fabrication of near-net shape products since they are widely used in form of sheets in marine, transport, and chemical engineering. The development of hot/cold rolling routes for the UFG metallic materials are very expensive due to much higher cost of the UFG metallic materials and time consuming due to numerous experimental trials. The objective of this work is to perform physical simulation of cold rolling of the UFG Al 5083 alloy obtained via equal channel angular pressing with parallel channels and to analyze the effect of cold rolling on the microstucture and microhardness of the material. It is demonstrated that physical simulation of metalforming processes for the UFG metallic materials can significantly reduce the amount of material required for development of processing routes and increase the efficiency of experimental work.

## 1. INTRODUCTION

Aluminium alloys play a very important role in modern engineering since they are the most used non-ferrous material. They have been widely used in various sectors of engineering due to their good corrosion resistance, good mechanical properties along with good machinability, weldability, and relatively low cost [1,2]. In recent years, much progress has been made in the studies on the ultra-fine grained (UFG) Al alloys for advanced structural and functional use associated both with the development of novel routes for the fabrication of bulk UFG and NS Al alloys using severe plastic deformation (SPD) techniques and with investigation of fundamental mechanisms leading to improved properties [3-5].

Among all Al alloys, the non-heat treatable Al-Mg-Mn alloys (Al alloys of the 5xxx series) are one of the most attractive Al alloys for marine and transport engineering as well as for the chemical industry [1]. A significant body of research on grain refinement in these Al alloys using 'bottom-up' approach, namely, (cryo)milling of powders followed by powder consolidation exists in the literature [6-15]. The 'top-down' approach to refine the microstructure of the Al-Mg-Mn alloys using SPD techniques is a more efficient way to fabricate high strength alloys, but less research on SPD

Corresponding author: M.Yu. Murashkin, e-mail: maxmur@mail.rb.ru

processing of the Al alloys of 5xxx series has been done [16 17]. It was demonstrated that equal channel angular pressing (ECAP) [18] is an efficient technique for grain refinement in the Al-Mg-Mn alloys in order to significantly improve their mechanical strength, though it results in degradation of their ductility [16,17]. Billets having a square or cylindrical cross section can be processed via ECAP. The Al-Mg-Mn alloys often have to undergo hot/cold rolling metalforming operations for fabrication of near-net shape products since they are often used in form of sheets. Thus, the hot/cold rolling routes need to be developed for the final metalforming operations on the UFG Al-Mg-Mn alloys. However, these metalforming operations can significantly affect the microstructure of the UFG Al-Mg-Mn alloys and, thus, change their properties. It should be also noted that the development of hot/cold rolling routes for the UFG metallic materials are very expensive due to their much higher cost, compared to the coarse-grained counterparts, and time consuming due to the numerous experimental trials to be carried out in order to find the optimal processing parameters. Physical simulation of metalforming processes can be utilized to minimize the amount of material for such experimental work as well as to increase the efficiency of experimental work and to reduce its cost. In physical simulation, a small amount of materials is subjected to the same thermo-mechanical profile that the real material undergoes during processing at industrial scale [19,20]. For example, the hot/cold rolling of large metal chalks at the industrial scale can be reproduced by plane strain compression testing of very small specimens at the lab scale since the material is deformed with the similar stress constraint [20]. If the simulation is accurate, the outcomes of physical simulation can be readily transferred from the laboratory to the full size production process. Thus, the major objective of the present work is to demonstrate that physical simulation of cold rolling of the UFG Al 5083 alloy can be a useful tool in order to analyze the effect of cold rolling on the microstructure and mechanical properties of the material in a very efficient manner and at low cost.

## 2. MATERIAL AND PROCESSING

An Al 5083 alloy (Al-4.4Mg-0.7Mn-0.15Cr wt.%) was chosen as a material for this investigation. The material was supplied in form of a hot rolled plate having a thickness of 100 mm. The as-received material was annealed at 350 °C for 2 h. The rods having a diameter of 18 mm and a length of 100 mm were machined and subjected to equal channel angular pressing with parallel channels (ECAP-PC). This method has been successfully applied for grain refinement in various Al alloys [21,22]. Schematic presentation of this processing technique is given in Fig. 1a and a detailed description of the technique can be found in [21,23]. The intersection angle between the parallel channels and the channel connecting them $\Phi$ was $110^{o}$ and the distance **K** was 20 mm (Fig. 1a). The bar was heated up to 180 °C in the furnace and soaked for 15 min followed by its lubrication and a processing pass in the ECAP-PC die heated to the same temperature. The punch speed was 6 mm/s. The bars were subjected to 7 ECAP-PC passes. The strain produced in each ECAP-PC pass was ~ 1.6, so the total cumulative strain induced into each sample was ~ 11.2.

## 3. EXPERIMENTAL PROCEDURES

Physical simulation of cold rolling was performed via plane strain compression testing in a thermo-mechanical simulator GLEEBLE 3800. Plane strain compression testing is a laboratory testing method which allows the measurement of the stress-strain behavior of metals and alloys to be carried out under controlled conditions of strain rate and temperature with constraint which are similar to those of industrial plate rolling [24,25]. The schematic representation of plane strain compression testing is given in Fig. 1b. Specimens in form of plates having dimensions of 20x15x5 $mm^3$ were machined from the processed rods. The 'rolling direction' (RD) in the specimens for physical simulation coincided with the pressing direction in the ECAP-PC processed samples as shown on Fig. 1c. Plane strain compression testing was carried out at room temperature with strain rate of 10 $s^{-1}$ at room temperature. The plates from ECAP-PC processed sample were subjected to plane strain compression testing to reduction ratios of 10%, 20%, 30%, and 40% with 10% reduction ratio per each step. The plates from the coarse-grained material were additionally deformed to the total reduction ratio of 50% with 10% reduction ratio per step. The break time between plane strain compression steps was 30 s which is relevant to that between rolling passes during real cold rolling of the material. It should be noted that no any formation of cracks was observed in the coarse-grained material after compression with the total reduction ratio of 50%, whereas some micro-cracks were present at the edges of the ECAP-PC processed samples after compression with the total reduction ratio of 40%. The flow stress $\sigma$ during

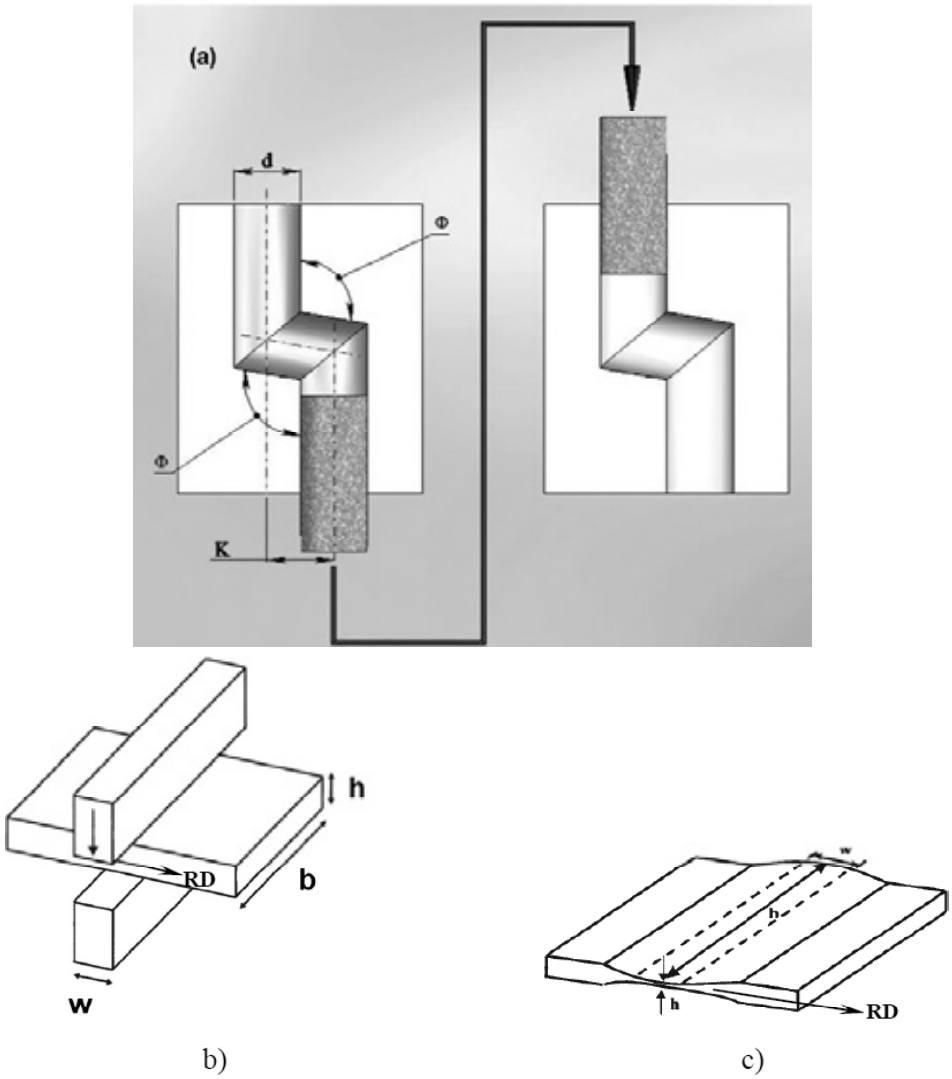


**Fig. 1.** a) Schematic presentation of the ECAP-PC processing technique; b) schematic presentation of plane strain compression test; b) schematic presentation of a sample after plane strain compression test.

plane strain compression testing was calculated as [26]

$$\sigma = \frac{\sqrt{3}}{2}\frac{F}{wL}, \tag{1}$$

where $F$ is the load, $w$ the width of the anvils, and $L$ the specimen width. True compressive strain was estimated as [26]

$$\varepsilon = \ln\left(\frac{h_0}{h}\right), \tag{2}$$

where $h_o$ is the initial thickness of the plate and $h$ the thickness of the plate during plane strain compression testing.

The microstructure of the as-received coarse-grained material was analyzed using optical microscope Olympus GX41. Samples for optical microscopy studies were prepared using standard metallographic technique. The samples were polished to the mirror-like surface using colloidal silica at the final stage. To reveal the grain structure, the samples were etched using the Keller reagent.

To study the microstructure evolution in the material during plane strain compression testing, transmission electron microscopy (TEM) analysis was carried out using a JEOL-2100 microscope operating at 200 kV. The microscope is equipped with a digital camera OLYMPUS D71. Samples for TEM study were cut out from the longitudinal section of the ECAP-PC processed samples and specimens after physical simulation of rolling and thinned down to ~ 100 μm. TEM foils were prepared by twin jet electro-polishing with 30% of Nitric acid in methanol at -25 °C at an operating voltage of 12 V. Observations were made in both the bright and

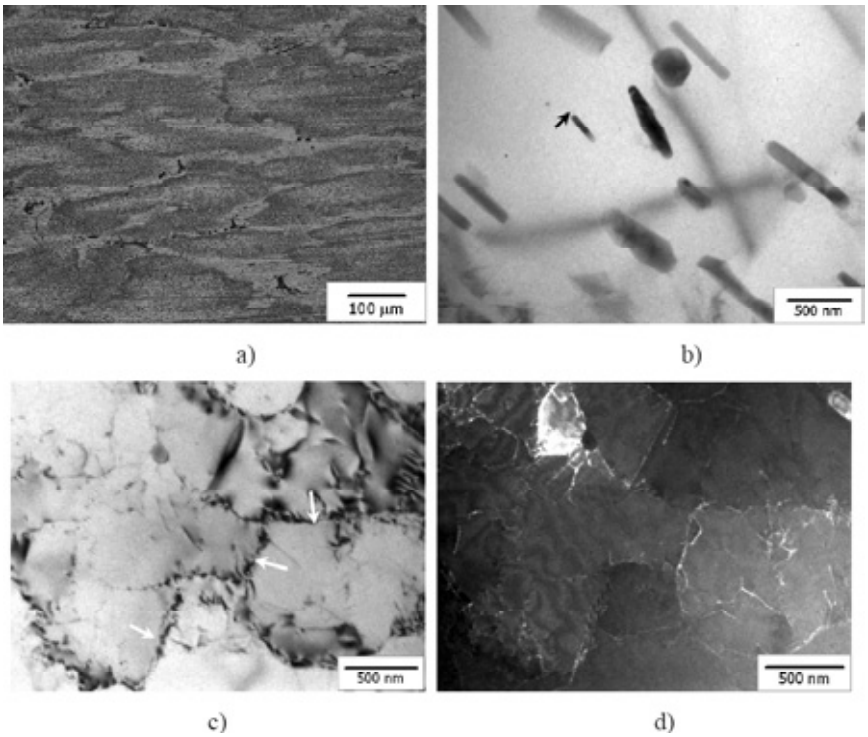


**Fig. 2**. Microstructure of the coarse-grained Al 5083 alloy: a) optical microscopy image, b) bright field TEM image illustrating dispersoids, c) bright field TEM image illustrating cell structure and dislocations, d) dark field TEM image illustrating cell structure and dislocations.

the dark field imaging modes, and selected area electron diffraction (SAED) patterns were recorded from the areas of interest using an aperture of 1 mm nominal diameter. The linear intercept method was used to estimate the size of grains/subgrains and the size of least 200 grains/subgrains was measured.

The XRD measurements were conducted using Rigaku Ultima IV diffractometer using Cu$K_\alpha$ radiation (30 kV and 20 mA). Values of lattice parameter *a*, coherent domain size $d_{XRD}$ and elastic microdistortion level $<\varepsilon^2>^{1/2}$ for the initial and tested plates were calculated via Rietveld refinement method using the MAUD software [27]. Dislocation density $\rho$ was estimated using Eq. (3) [28]

$$\rho = 2\sqrt{3}\left\langle \varepsilon^2 \right\rangle^{1/2} / \left(D \times b\right), \quad (3)$$

where $\boldsymbol{b}$ is the Burgers vector ($\boldsymbol{b} = a\sqrt{2}/2$ for fcc metals) and *D* the size of the coherent scattering domain (CSD).

Microhardness of the material was measured using SHIMADZU HMV-2 microhardness tester equipped with Vickers diamond indenter. The load of 1 N was applied for 10 s. Ten measurements were carried out in the midsection of each sample, the average values of microhardness and their standard deviation were calculated.

## 4. RESULTS AND DISCUSSIONS

### 4.1. The effect of equal channel angular pressing on the microstructure of the Al 5083 alloys

Fig. 2 illustrates microstructure of the as-received hot rolled Al 5083 alloy after annealing. A homogeneous microstructure consisting of elongated grains having a length of 300...400 μm and a width of 100...200 μm is observed. The grains are elongated in the rolling direction (Fig. 2a). TEM analysis revealed that coarse grains subdivided into smaller cells with thin dislocation walls as boundaries (marked by white arrows on Fig. 2c). The cells have an equiaxed shape and their size is in the range of 0.5…1 μm. The interior of cells is free of dislocations. Misorientation across these cells appears to be small since many of the subgrains show a similar contrast under a certain diffraction condition (Fig. 2d) though a few individual cells demonstrating different contrast are also visible (marked by black arrow on Fig. 2d). Such microstructure was developed during hot rolling of the material and its further annealing: A great number of dislocations generated during hot rolling was able to rearrange so as to form such stable configurations because of the

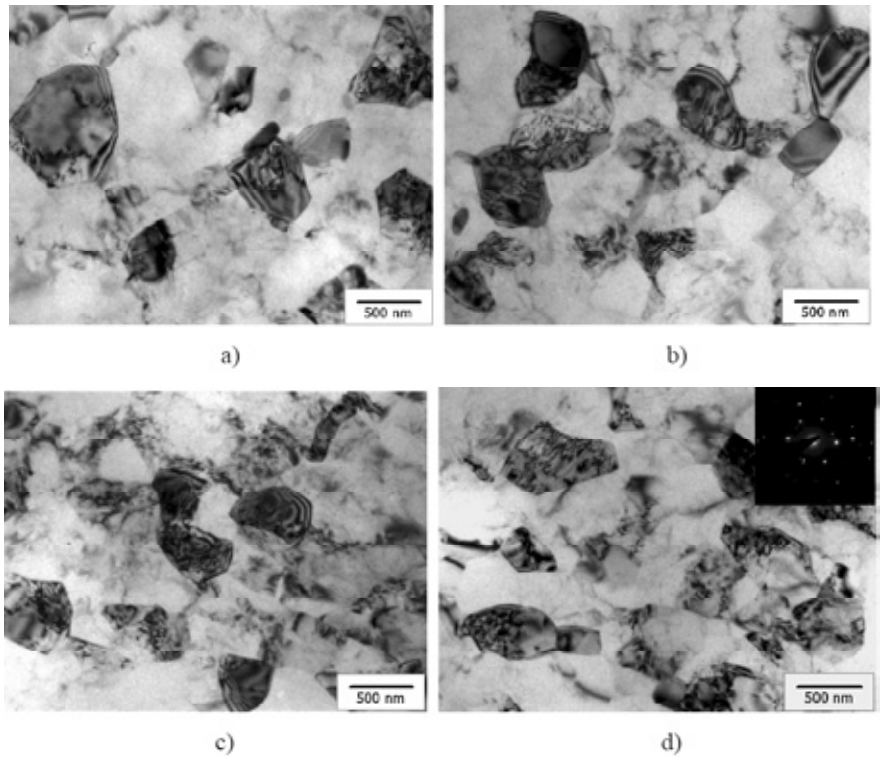


**Fig. 3**. Bright field TEM images of the Al 5083 alloy after ECAP-PC processing at 180 °C for 7 passes: a, b) transversal section, c, d) longitudinal section.

enhanced frequency of cross-slip and climb, and further annealing led to annihilation of the statistically stored dislocation in the interior of cells via their climb [36]. It should be noted that the rod type second phase precipitates having a length of 400...600 nm and a width of 80...120 nm are also present in the microstructure and can be identified as AlMnCr dispersoids typically present in the Al-Mg-Mn alloys (Fig. 2b) [1].

ECAP-PC processing of the material led to formation of a very homogeneous UFG microstructure (Fig. 3). Majority of ultra-fine grains have an equiaxed shape and their size is in the range of 250...600 nm with the average size of 480 nm (Fig. 3). Lattice dislocations are present in the interior of most of the ultra-fine grains. The X-Ray measurements have clearly demonstrated that dislocation density after ECAP-PC processing has increased by two orders of magnitude (Table 1). Finer spherical dispersoids having a size of 50...100 nm are observed in the microstructure. As well known, ECAP processing of the Al alloys can lead to fragmentation of second phase particles and dispersoids if they have a rod shape as a result of shearing processes [29-31]. It should be also noted that the ECAP-PC processing reduced the CSD size by a factor of 3 (Table 1)

**Table 1.** Results of the X-Ray studies of the coarse-grained and UFG Al 5083 alloy before and after plane strain compression testing.

| | Reduction ratio | CSD [nm] | $<\varepsilon^2>^{1/2}$ [%] | Lattice parameter [*a*] | $\rho$ [$m^{-2}$] |
|---|---|---|---|---|---|
| CG | Non rolled | 480 ± 34 | 0.0004 ± 0.00002 | 4.0716 ± 0.0005 | $1.01 \times 10^{11}$ |
| | 10% | 244 ± 12 | 0.0820 ± 0.0018 | 4.0701 ± 0.0008 | $4.09 \times 10^{13}$ |
| | 30% | 240 ± 35 | 0.1100 ± 0.0048 | 4.0689 ± 0.0010 | $5.59 \times 10^{13}$ |
| | 50% | 239 ± 28 | 0.1100 ± 0.0064 | 4.0689 ± 0.0009 | $5.62 \times 10^{13}$ |
| UFG | Non rolled | 157 ± 10 | 0.0520 ± 0.0007 | 4.0711 ± 0.0001 | $4.04 \times 10^{13}$ |
| | 10% | 109 ± 12 | 0.0880 ± 0.0024 | 4.0724 ± 0.0002 | $9.85 \times 10^{13}$ |
| | 30% | 100 ± 17 | 0.0110 ± 0.0070 | 4.0709 ± 0.0009 | $1.34 \times 10^{14}$ |
| | 40% | 96 ± 10 | 0,0130 ± 0,0029 | 4,0701 ± 0,0007 | $1,65 \times 10^{14}$ |

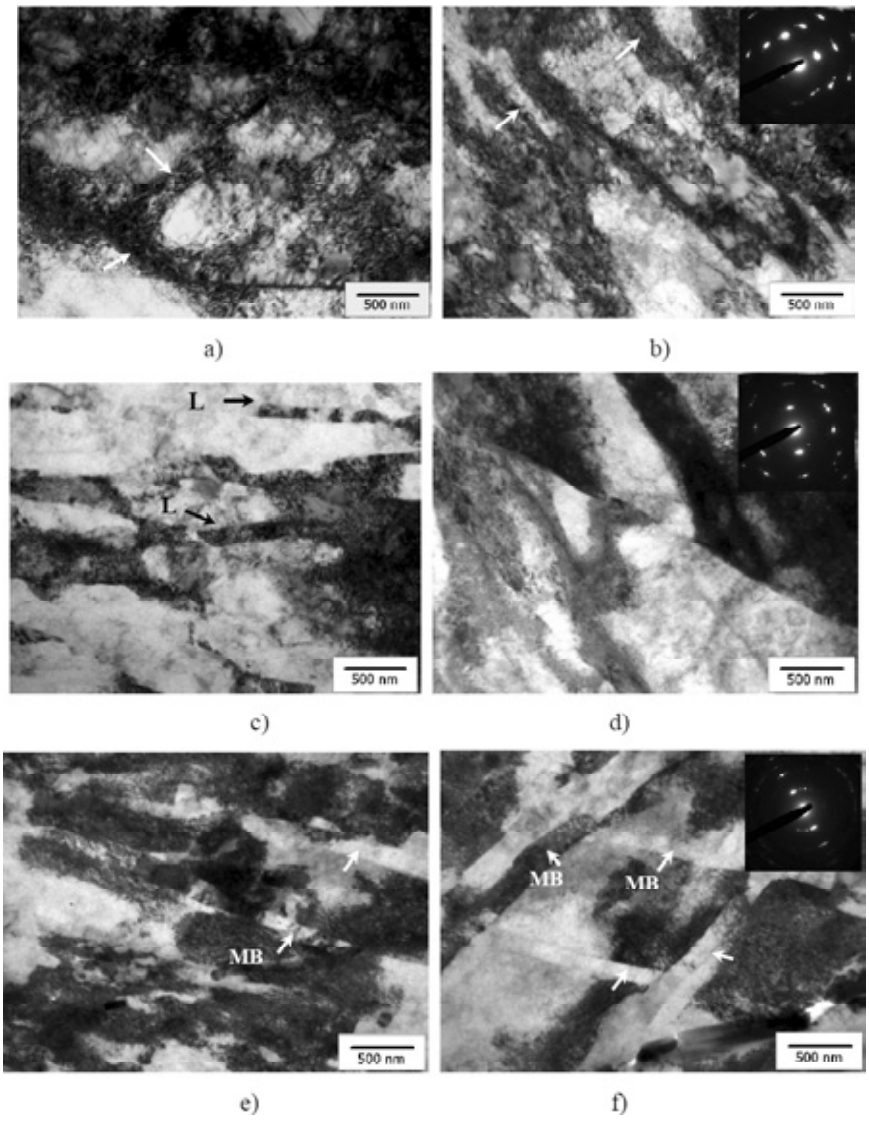


**Fig. 4**. TEM images of the coarse-grained Al 5083 alloy after plane strain compression testing with reduction ratio of: a, b) 10%, c,d) 30%, e,f) 50%.

due to formation of much finer microstructure as well as due to the significant increase of lattice dislocation density (Table 1).

## 4.2. Evolution of microstructure in the Al 5083 alloy during plane strain compression testing

### 4.2.1. Evolution of microstructure in the coarse-grained material

Fig. 4 illustrates evolution of microstructure in the coarse-grained Al 5083 alloy during plane strain compression testing at room temperature. Formation of equiaxed cells having a size of 0.5...1 μm is observed after deformation to true compressive strain of ~ 0.11 (reduction ratio of 10 %). The individual cells are separated by relatively diffuse single dense dislocation walls (DDWs) marked by white arrows on Fig. 4a. The width of DDWs is in the range of 100...120 nm (Fig. 4a). Areas of micro banding (MB) consisting of very elongated cells are also observed (marked on Fig. 4b). They have a width of 100...150 nm. An increase of true compressive strain to ~ 0.36 (reduction ratio of 30%) leads to formation of a more complex microstructure consisting of lamellae having a length of 0.5...2 μm and a width of 150...200 nm (marked as 'L' on Fig. 4c) and elongated cells. The lamellae boundaries are parallel to the rolling plane (Fig. 4c). With increasing true compressive strain to ~0.69 (reduction ratio of 50%), a great number of MBs developed in the material and some of them formed clusters consisting of a 2-3 layers (Figs. 4e and 4f). Some of the MBs in these clusters have different

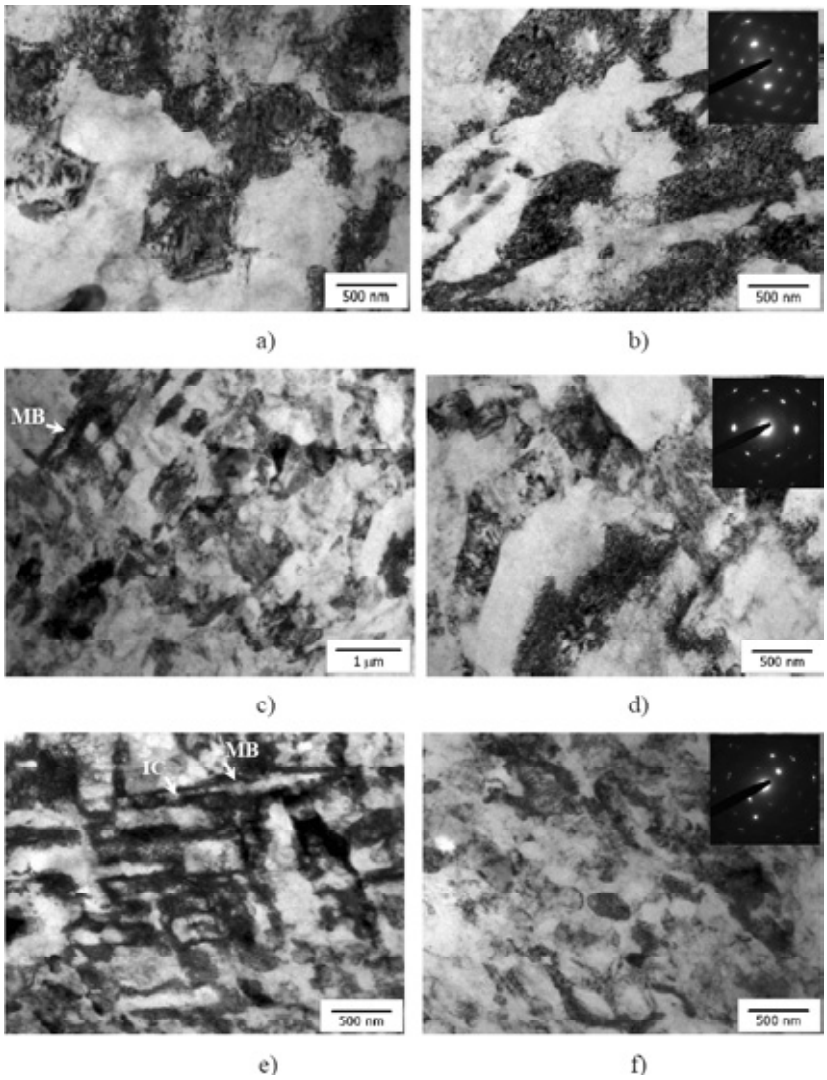


**Fig. 5**. Bright field TEM images of the UFG Al 5083 alloy after plane strain compression testing with reduction ratio of: a,b) 10%, c,d) 30%, e,f) 40%.

contrast suggesting the presence of large misorientation between them (Fig. 4f). These MBs have a width of 100...200 nm, they are spaced at 0.6...1 μm (Figs. 4e and 4f) and intersected at angles of 60...75° (Fig. 4f). No significant effect of dispersoids on the microstructure evolution during plane strain compression testing of the coarse-grained Al 5083 alloy at room temperature was observed.

It should be noted that the size and shape of the cells formed after plane strain compression testing to low strains (Figs. 2a and 2b) is very similar to those observed in the coarse-grained material though the latter had much thinner cell walls (Fig. 2b). The X-Ray measurements of the coarse-grained specimens also confirm that the CSD size is not significantly affected by the true compressive strain (reduction ratio) (Table 1). So, it can be assumed that the initial microstructure can play an important role in the formation of the microstructure during cold rolling. An increase of dislocation density in the cell interior with increasing true compressive strain is clearly observed on the TEM images (Fig. 4), and it is also confirmed by the results of the X-Ray analysis (Table 1). It should be noted that there is a significant body of experimental and theoretical research on microstructure evolution in the Al alloys during their cold rolling, and the nearly complete theory of this process has already been developed [32-40]. Our observations of the microstructure evolution during cold plane strain compression testing of the Al5083 alloy are in a very good accordance with the literature data, thus, indicating the correctness of application of physical simulation to study the microstructure evolution during cold rolling of the Al alloys.

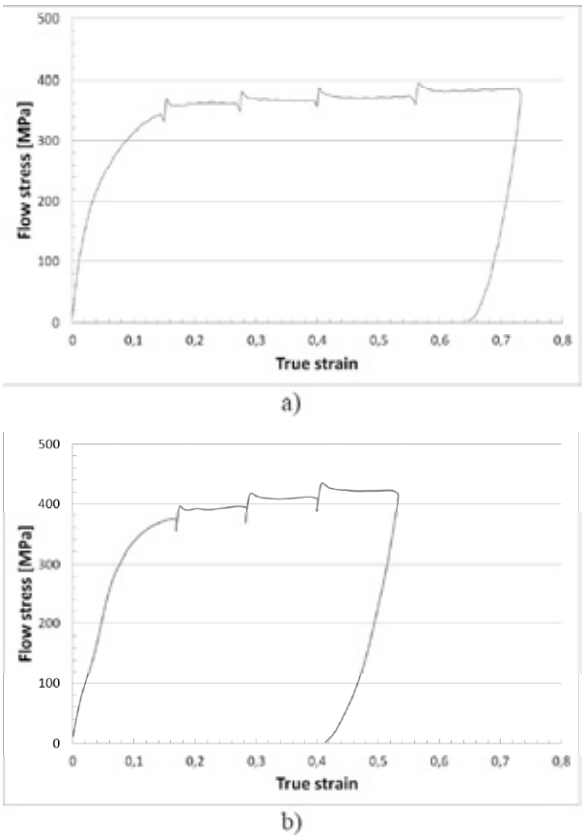


**Fig. 6**. Experimental flow stress - true compressive strain from plane strain compression testing of the Al 5083 alloy in: a) coarse-grained condition, b) UFG condition.

### 4.2.2. Evolution of microstructure in the ultra-fine grained material

Microstructure evolution during plane strain compression testing of the UFG Al 5083 at room temperature (Fig. 5) significantly differs from that observed in its coarse-grained counterpart (Fig. 4). First, no formation of cell microstructure in the grain interior is observed during plane strain compression testing. After deformation to compressive strain of ~ 0.11 (reduction ratio of 10%), some ultra-fine grains tend to elongate along the 'rolling direction' (Fig. 5b), but most of the grains retain their equi-axed shape (Fig. 5a). With increasing compressive strain to ~ 0.36 (reduction ratio of 30%), formation of individual MBs is observed in the microstructure (Fig. 5c) and most of the ultra-fine grains are elongated along the rolling direction (Fig. 5d). No lamellae-type microstructure is seen. Higher dislocation density is observed in the interior of ultra-fine grains (Fig. 5d), it increases by order of magnitude (Table 1). Further increase of true compressive strain to ~ 0.51 (reduction ratio of 40%) results in bi-modal microstructure consisting of areas containing

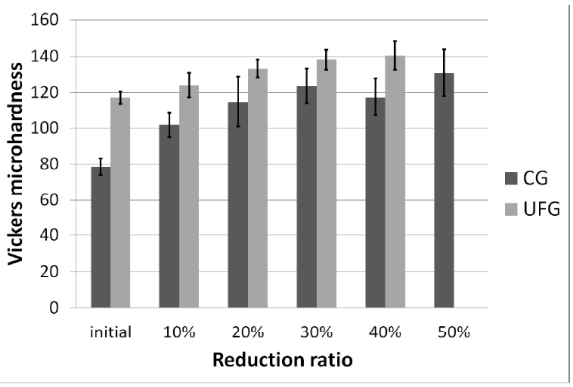


**Fig. 7**. Effect of plane strain compression testing on the Vickers microhardness of coarse-grained and UFG Al5083 alloy (measurements are taken from the midsection of the tested specimens).

significant amount of MBs (Fig. 5e) and areas where elongated ultra-fine grains prevail (Fig. 5f). Unlike in the coarse-grained material, formation of equiaxed cells with very diffuse cell boundaries can be observed within come MBs in the UFG Al 5083 alloy (Fig. 5e). Qualitative analysis of the microstructure shows much lower density of MBs in the UFG material (Figs. 5e and 5f) compared to that in the coarse-grained material (Fig. 4e and 4f). No significant effect of fine dispersoids on the microstructure evolution in the UFG Al 5083 can be noted: No any specific microstructural features are seen in vicinity of the dispersoids.

## 4.3. The effect of ECAP-PC processing and plane strain compression testing on the flow stress and microhardness of the coarse-grained and UFG Al 5083 alloy

Fig. 6 demonstrates the experimental flow stress - true strain curves from plane strain compression testing of both coarse-grained and UFG material. It is seen from the curves that grain refinement in the Al 5083 leads to increased flow stress during plane strain compression testing. For example, the UFG material in the 4th 'rolling pass' shows flow stress of 421 MPa (Fig. 6b), whereas the CG material in the same rolling pass is deformed under 368 MPa (Fig. 6a). Flow stress tends to increase with true compressive strain (reduction ratio) in both CG and UFG material (Fig. 6). Analysis of the X-Ray results (Table 1) along with TEM data (Sections 3.2.1 and 3.2.2) leads to conclusion that different hardenings mechanisms are responsible for the strengthening

of the CG and UFG materials. Formation of lamellar-type microstructure with ultra-fine lamellae and high fraction of micro-shear bands (Section 3.2.1) seems to be the main mechanism for hardening of the CG material, since dislocation density does not increase significantly with reduction ratio as seen from Table 1. The can be related to rearrangement of dislocations generated during plane strain compression testing and their significant contribution to formation cells boundaries, MBs, etc. On the contrary, dislocation density increases by one order of magnitude during plane strain compression testing (Table 1), thus, providing significant dislocation strengthening [41]. Dislocations generated during plane strain compression testing of the UFG material to low true compressive strains ($\leq$0.36) mainly provided plastic deformation of individual ultra-fine grains. The results of microhardness measurements (Fig. 7) are in a good agreement with the stress-strain curves (Fig. 6). It is clearly seen that the Vickers microhardness tends to increase with reduction ratio in both CG and UFG materials. No tendency to saturation of the Vickers microhardness is observed in both conditions. Thus, it can be concluded that cold rolling of the Al 5083 alloy in both conditions to higher reduction ratios can lead to further material hardening.

### 4.4. Advantages of application of physical simulation for development of thermo-mechanical processing routes for the UFG metallic materials

Significant amount of large-scale trials is usually required for development of advanced thermo-mechanical processing routes for fabrication of the UFG metallic materials. For example, this is clearly seen from [42], where whole ECAP processed UFG CP Ti specimens were subjected to cold rolling route in order to analyze its effect on the microstructure, thermal stability, and mechanical properties of the UFG material. Recently, it was also shown that many UFG metallic materials such as IF steel [43], commercially pure CP Cu [44], CP Al [45] demonstrate high bi-axial stretch formability similar to that of their coarse-grained counterparts. So these UFG metallic materials can undergo additional metalforming operations for fabrication of complex shape tools and have a potential for application in various engineering sectors [46]. Since these metalforming operations might significantly affect their microstructure and mechanical properties, development of processing path will take significant amount of experimental trials and research using significant amount of expensive UFG material.

This work clearly shows that physical simulation of the metalforming operation can significantly reduce the amount of material required for experimental trials as well as to increase efficiency of experimental work. First, precise data on stress strain behavior of the material during cold rolling can be recorded and the load on the rolling mills can be predicted. This is very important in order to avoid the damage of the rolling mills since some UFG metallic materials can demonstrate superior mechanical strength and enhanced strain rate sensitivity resulting in extremely high flow stresses if they are deformed at high strain rates [5]. Second, the processing parameters (temperature, reduction ratio, strain rate) can be perfectly controlled in the thermo-mechanical simulator. So the effect of the rolling parameters on the microstructure, texture, mechanical strength and any other functional properties can be easily determined via analysis of small specimens subjected to plane strain compression testing. The results thus obtained from physical simulation can be readily transferred into larger fabrication scale.

## 5. CONCLUSIONS

A coarse-grained Al 5083 alloys is subjected to equal channel angular pressing with parallel channels (ECAP-PC) at 180 °C for 7 passes resulting in formation of a homogeneous microstructure consisting mainly of equiaxed ultra-fine grains having the average size of 480 nm. Physical simulation of cold rolling of both coarse-grained and ultra-fine grained (UFG) Al 5083 alloy is performed via plane strain compression testing at room temperature in a thermo-mechanical simulator. Evolution of microstructure and hardness of both material's conditions during plane strain compression testing is performed. It is demonstrated that:

1) Evolution of microstructure during plane strain compression testing of the coarse-grained Al 5083 alloy is very similar to that reported earlier for various coarse-grained Al-Mg alloys during their cold rolling.
2) Evolution of microstructure in the UFG Al 5083 alloy during plane strain compression testing is very different from that observed in its coarse-grained counterpart.
3) Cold rolling of both coarse-grained and UFG material leads to increase of their mechanical strength with true strain induced into specimens.

4) Physical simulation of cold rolling of UFG metallic materials is a very convenient tool that allows to predict microstructure and properties of the material after its rolling in efficient manner at lower cost.

## ACKNOWLEDGEMENTS

MYuM, IS, and VUK would like to acknowledge gratefully the Russian Ministry for Education and Science for the financial support of this study through the Federal Targeted Program: Contract N° 14.B37.21.1953 by 14 November 2012. NAE and RZV thank the Russian Ministry for Education and Science for funding through Contract N° 14.B25.31.0017 by 28 June 2013. IS also acknowledges gratefully the Spanish Ministry of Economy and Competitiveness for financial support through the Ramon y Cajal Fellowship.

## REFERENCES

[1] *Handbook of Aluminium*, ed. by G.E. Totten and D.S. MacKenzie (Marcel Dekker, USA, 2003).
[2] I.J. Polmear, *Light Alloys: From traditional alloys to nanocrystals* (Elsevier, Oxford, 2006).
[3] I. Sabirov, M.Yu. Murashkin and R.Z. Valiev // *Mater. Sci. Eng. A*. **560** (2013) 1.
[4] Y. Estrin, M.Yu. Murashkin and R.Z. Valiev, In: *Fundamentals of aluminium metallurgy: Production, processing and applications*, ed. by R. Lumley (Woodhead Publishing Limited, Cambridge, 2010), p. 468.
[5] T.G. Langdon // *Acta Mater.* **61** (2013) 7035.
[6] T.D. Topping, B. Ahn, Y. Li, S.R. Nutt and E.J. Lavernia // *Metall. Mater. Trans. A* **43** (2012) 505.
[7] B.Q. Han, Z. Lee, S.R. Nutt, E.J. Lavernia and F.A. Mohamed // *Metall. Mater. Trans. A.* **34** (2003) 603.
[8] A.P. Newbery, B. Ahn, T.D. Topping, P.S. Pao, S.R. Nutt and E.J. Lavernia // *J. Mater. Proc. Tech.* **203** (2008) 37.
[9] Z. Lee, V. Radmilovic, B. Ahn, E.J. Lavernia and S.R. Nutt // *Metal. Mater. Trans. A* **41** (2010) 795.
[10] D.B. Witkin and E.J. Lavernia // *Prog. Mater. Sci.* **51** (2006) 1.
[11] D. Witkin, Z. Lee, R. Rodriguez, S. Nutt and E. Lavernia // *Scr. Mater*. **49** (2003) 297.
[12] B.Q. Han, Z. Lee, D. Witkin, S. Nutt and E.J. Lavernia // *Metall. Mater. Trans. A.* **36** (2005) 957.
[13] D. Witkin, B.Q. Han and E.J. Lavernia // *Metall. Mater. Trans. A.* **37** (2006) 185.
[14] G.J. Fan, H. Choo, P.K. Liaw and E.J. Lavernia // *Acta Mater*. **54** (2006) 1759.
[15] Z. Lee, D.B. Witkin, V. Radmilovic, E.J. Lavernia and S.R. Nutt // *Mater. Sci. Eng. A.* **410–411** (2005) 462.
[16] M.V. Markushev and M.Yu. Murashkin // *Phys Metal Metall.* **98** (2004) 1.
[17] M.V. Markushev, C.C. Bampoton, M.Yu. Murashkin and D.A. Hardwick // *Mater. Sci. Eng. A* **234–236** (1997) 927.
[18] R.Z. Valiev and T.G. Langdon // *Prog. Mater. Sci.* **51** (2006) 881.
[19] D. Ferguson, W. Chen, T. Bonesteel and J. Vosburgh // *Mater. Sci. Eng. A* **499** (2009) 329.
[20] S.T. Mandziej // *Mater. Tech*. **44** (2010) 105.
[21] M.Yu. Murashkin, I. Sabirov, V.U. Kazykhanov, E.V. Bobruk, A.A. Dubravina and R.Z. Valiev // *J. Mater. Sci.* **48** (2013) 4501.
[22] E.V. Bobruk, M.Yu. Murashkin, V.U. Kazykhanov and R.Z. Valiev // *Rev. Adv. Mater. Sci.* **31** (2012) 14.
[23] G.I. Raab // *Mater. Sci. Eng. A* **410-411** (2005) 230.
[24] H. Shi, A.J. McLaren, C.M. Sellars, R. Shahani and R. Bolingbroke // *J. Test. Eval.* **25** (1997) 61.
[25] J.H. Beynon and C.M. Sellars // *J. Test. Eval.* **13** (1985) 28.
[26] S. Hosford // *Acta Metall.* **14** (1966) 1085.
[27] L. Lutterotti, S. Matthies and H.R. Wenk, In: *Proceeding of the 12th International Conference on Textures of Materials* (ICOTOM-12) **1** (1999) 1599.
[28] G.K. Williamson and R.E. Smallman // *Phil. Mag.* **1** (1956) 34.
[29] H.J. Roven, M. Liu and J.C. Werenskiold // *Mater. Sci. Eng. A*. **483–484** (2008) 54.
[30] P. Szczygiel, H.J. Roven and O. Reiso // *Mater. Sci. Eng. A.* **410** (2005) 261.
[31] C. Xu, M. Furukawa, Z. Horita and T.G. Langdon // *Acta Mater.* **51** (2003) 6139.
[32] D.A. Hughes and N. Hansen // *Metall. Trans. A.* **24** (1993) 2021.
[33] Q. Liu and N. Hansen // *Scripta Mater.* **32** (1995) 1289.
[34] D.A. Hughes and N. Hansen // *Acta Mater.* **45** (1997) 3871.
[35] Q. Liu, X. Huang, D.J. Lloyd and N. Hansen // *Acta Mater.* **50** (2002) 3789.
[36] D. Kuhlmann-Wilsdorf and N. Hansen // *Scr. Metall. Mater.* **25** (1991) 1557.

[37] D. Duly, G.J. Baxter, H.R. Shercliff, J.A. Whiteman, C.M. Sellars and M.F. Ashby // *Acta Mater*. **44** (1996) 2947.
[38] Y. Nakayama and K. Morii // *Acta Metall*. **35** (1987) 1747.
[39] D.A. Hughes, Q. Liu, D.C. Chrzan and N. Hansen // *Acta Mater*. **45** (1997) 105.
[40] D.A. Hughes and N. Hansen // *Acta Mater.* **45** (1997) 3871.
[41] M.F. Ashby // Phil. Mag. **21** (1970) 399.
[42] V.V. Stolyarov, L. Zeipper, B. Mingler, M. Zehetbauer // *Mater. Sci. Eng. A*. **476** (2008) 98.
[43] R. Yoda, K. Shibata, T. Morimitsu, D. Terada and N. Tsuji // *Scr. Mater.* **65** (2011) 175.
[44] E.C. Moreno-Valle, M.A. Monclus, J.M. Molina-Aldareguia, N. Enikeev and I. Sabirov // *Metal. Mater. Trans. A*. **44** (2013) 2399.
[45] A. Taylor, M. Weiss, T. Hilditch, N. Stanford and P.D. Hodgson // *Mater. Sci. Eng. A.* **555** (2012) 148-153.
[46] R.Z. Valiev, I. Sabirov, A.P. Zhilyaev and T.G. Langdon // J*OM* **64** (2012) 1134.